MATEC Web of Conferences **406**, 06002 (2024) https://doi.org/10.1051/matecconf/202440606002
2024 RAPDASA-RobMech-PRASA-AMI Conference

Effect of Pd substitution on elastic and lattice dynamic properties of B2 $Ti_{50}Ru_{50}$ – ab initio study

Bongani Ngobe[1, 2,*], *Mahlaga* Molepo[2], *Donald* Mkhonto[1], and *Maje* Phasha[1]

[1]Advanced Materials Division, MINTEK, Randburg, South Africa
[2]School of Physics, University of the Witwatersrand, Johannesburg, South Africa

Abstract. Owing to Nitinol's success, shape memory alloys (SMAs) enjoy unwavering attention as key futuristic intelligent structural materials. Despite the excellent shape memory effect (SME) and pseudo-elasticity, Nitinol is susceptible to high-temperature applications. Extensive research has been conducted to discover SMAs with improved higher-temperature properties by considering PGM-bearing B2 Ti-based compounds. In this study, the impact of palladium (Pd) addition on $Ti_{50}Ru_{50}$ to yield $Ti_{50}Ru_{50-x}Pd_x$ ternary compounds with martensitic transformation (MT) was investigated by employing a supercell approach. With the addition of Pd up to 25 at. %, B2 $Ti_{50}Ru_{50-x}Pd_x$ remained stable ($C_{11}>C_{12}$), while ternaries with Pd ≥ 31.25 at. % were found unstable ($C_{11}<C_{12}$).

1 Introduction

For the past 60 years, Nitinol-based SMAs have maintained their status as dominant smart materials of choice, due to their unmatched mechanical properties that outperform other shape memory alloys. The exceptional mechanical attributes of Nitinol-based SMAs have solidified their position as the dominant smart material of choice for over 60 years, surpassing the capabilities of other shape memory alloys. SMAs are widely used to create intelligent devices and tools owing to their high energy density, actuation strain, and large strain recovery [1-2]. SMA's intelligence arises from their exceptional ability to transform between a high-temperature B2 phase and multiple low-temperature martensitic phases, such as B19, B19', and $L1_0$ [1-2]. The B19 phase with an orthorhombic crystal structure is found in TiAu, TiPd, and TiPt systems; the B19' phase with a monoclinic crystal structure, is associated with the TiNi system while the $L1_0$ phase with a tetragonal crystal structure is associated with TiIr system [1, 3]. Despite the remarkable properties of these materials, such as martensitic transformation (MT), discovered in the early 1930s, SMAs were only considered for technological applications in aeronautic and medical industries in the 1960s and 1970s, mainly owed to breakthroughs in TiNi [2, 4]. The martensitic transformation (MT) is a key characteristic inherent to SMAs that govern the shape memory effect (SME), a unique behaviour observed in these functional materials [2, 4].

* Corresponding author: Bonganing@mintek.co.za & 2623288@students.wits.ac.za

Nitinol, despite its limitation on structural applications exceeding 400 K, remains the preferred smart material due to its outstanding shape memory effect and pseudo-elastic properties [1]. Meanwhile, other shape memory alloys like TiPd and TiPt, which exhibit a B2 structure and are based on titanium and precious group metals, have been investigated for high-temperature applications above 400 K, such as in sensors and actuators for jet engines and core exhaust chevron systems [5-7].

In the structural family of B2 Ti-PGMs compounds, there exists the TiRu alloy, which nucleates instantly from a liquidus state to form a Cesium Chloride (CsCl) phase near equiatomic composition during the cooling and solidification process [3, 8]. In contrast to all B2 compounds listed above, the TiRu B2 phase remains stable down to room temperature, without undergoing any martensitic transformation [9].

The martensite transformation happens within a narrow chemical composition range of certain metallic compounds, such as in the CsCl intermetallic compounds formed between group 4 and 10 transition elements at near equiatomic compositions [10]. The authors previously conducted a systematic study on the effects of Ni, Pd, and Pt additions to B2 TiRu, employing the virtual crystal approximation (VCA) method, to induce diffusionless martensitic transformations. The method was used to carry out the Ru pseudo atom mixing with Ni, Pd, and Pt at a fractional compositional variation of 2.5 at. %, to yield $Ti(Ru_{1-x}TM_x)$ ternary compositions [10-11]. In addition, the current authors used the supercell (SC) method to study and report the impact of Ni and Pt alloying on the ordered B2 TiRu [12-13].

To meet the comprehensive objective of the study on the effect of adding group VIII (Ni, Pd, and Pt) transition metals to induce MT in B2 TiRu, this current study investigates and reports the effect of Pd. A 2x2x2 B2 TiRu supercell was constructed, to enable the substitution of some of the Ru atoms with Pd atoms at intervals of 6.25 at. %. The substitution was performed in a compositional range of 6.25 to 50 at. % to yield $Ti_{50}Ru_{50-x}Pd_x$ ternary alloy compositions.

2 Computational methods

This study utilized the Cambridge Serial Total Energy Package (CASTEP) code, which is based on density functional theory (DFT) [14-15], to compute all reported predictions. CASTEP is integrated into the Materials Studio software and employs the plane-wave pseudopotential method (PAW) [16]. The calculations used ultra-soft pseudopotentials (USPPs) to simulate electron-ion interactions [16] and the Perdew-Burke-Ernzerhof (PBE) functional within the generalized gradient approximation (GGA) to describe electron exchange and correlation effects [17].

The convergence was attained for the binary $Ti_{50}Ru_{50}$ and $Ti_{50}Pd_{50}$ B2 unit cells using a 500 eV energy cut-off and 13×13×13 k-points mesh, which yielded satisfactory total energy results. Meanwhile, for the ternary $Ti_{50}Ru_{50-x}Pd_x$ systems in a 2×2×2 supercell, a 7×7×7 k-points grid was used. This 2×2×2 supercell comprised of 16 atoms represents the ternary crystal structure of B2 $Ti_8Ru_{8-x}Pd_x$. To achieve optimal accuracy and reliability, the investigated B2 crystal structures were optimized using BFGS minimization [18] with robust convergence criteria: 1×10-5 eV/atom energy tolerance, 0.03 eV/Å residual forces, 0.05 GPa bulk stress, and 1×10-3 Å atomic displacement. At elevated temperatures, the TiRu B2 phase crystallizes in a cubic CsCl-type structure (Pm-3m space group, No. 221), characterized by lattice parameters a = b = c = 3.076 Å. The Ti and Ru atoms are situated at 1b (0.5, 0.5, 0.5) and 1a (0, 0, 0) positions, respectively [9].

Fig. 1 below illustrates the B2 crystal models employed to assess investigated compounds' stability characteristics (structural, thermodynamic, mechanical, and vibrational).

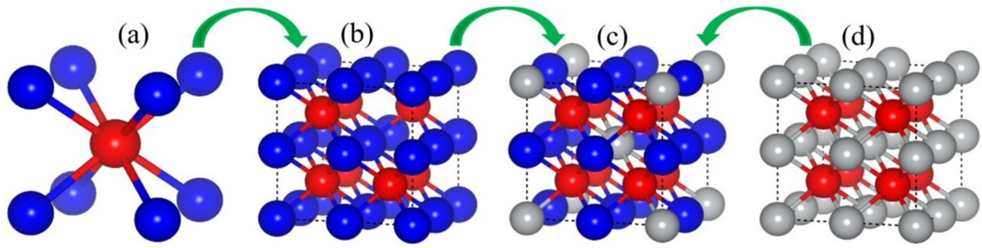

Fig. 1. Crystal structures of (a) B2 TiRu unit and its 2×2×2 supercell expansions: (b) Ti_8Ru_8, (c) $Ti_8Ru_{8-x}Pd_x$, and (d) Ti_8Pd_8.

3 Results and discussion

3.1 The structural and thermodynamic properties

Thermodynamic properties are fundamental for comprehending material behaviour, including predicting the feasibility of achieving a preferred alloy composition in a specific phase and assessing its stability for intended use [19]. Table 1 shows the ground state and thermodynamic properties reported in this study. The properties reported in this study were computed from geometrically relaxed crystal structures, permitting the unit cell volume and internal stress adjustments to achieve an equilibrium state. The results show consistency with previous findings of other authors [9, 20-21], specifically for the $Ti_{50}Ru_{50}$ and $Ti_{50}Pd_{50}$ binary systems. The data in Table 1, indicate a linear relationship between the Pd concentration and lattice parameters in ternary alloys. The above is evidence of the subsequent crystal structure expansion because Pd has a larger atomic radius (1.37 Å) than Ruthenium (1.34 Å). This expansion is further reflected in the volume increase as shown in Table 1.

Table 1. Calculated parameters of investigated compounds in their equilibrium state, with literature values in parenthesis.

B2 compounds	**Structural properties**		
	Lattice parameters, *a* (Å)	Enthalpies of formation, ΔH_F (eV/atom)	Volume (Å^3)
$Ti_{50}Ru_{50}$	3.08 [3.08][9]	-0.76 [-0.77][20]	233.75
$Ti_{50}Ru_{43.75}Pd_{6.25}$	3.09	-0.70	235.85
$Ti_{50}Ru_{37.5}Pd_{12.5}$	3.10	-0.65	238.11
$Ti_{50}Ru_{31.25}Pd_{18.75}$	3.11	-0.61	240.71
$Ti_{50}Ru_{25}Pd_{25}$	3.12	-0.60	243.06
$Ti_{50}Ru_{18.75}Pd_{31.25}$	3.13	-0.55	245.98
$Ti_{50}Ru_{12.5}Pd_{37.5}$	3.14	-0.53	248.25
$Ti_{50}Ru_{6.25}Pd_{43.75}$	3.15	-0.51	251.11
$Ti_{50}Pd_{50}$	3.17 [3.17][21]	-0.49[-0.45][21]	253.97

The enthalpy of formation (ΔH_F), defined in Equation 1 [22], represents a critical physical property quantifying the energy difference between a compound and its constituent elements. It represents the thermodynamic potential of the compound to form from its alloying elements.

$$\Delta H_F = E_T - \sum_i x_i E_i \, , \tag{1}$$

In this equation, E_T denotes the compound's total energy, while E_i denotes the energy of each element i in its stable ground-state crystal structure, present at a concentration of x_i atomic percentage. A compound is said to be thermodynamically stable when its enthalpy of formation has the most negative $(\Delta H_F > 0)$ value, with a less negative value rendering the compound unstable at 0 K [9]. Table 1 lists the computationally predicted enthalpies of formation for investigated B2 compounds, and all the investigated compounds exhibit negative values. All demonstrate their relative thermodynamic stability is lower than the reference compound, $Ti_{50}Ru_{50}$ (-0.76 eV/atom).

3.2 The elastic properties

Understanding a material's elastic constants is crucial, they reveal key facets of its behaviour, including the nature of its atomic bonds, its anisotropic properties, its ability to withstand mechanical stress and its overall rigidity [9].

Born-Huang's lattice dynamical theory [9, 23-24] provides a framework to evaluate the mechanical stability of crystals. It states that for a cubic system C_{11}, C_{12} and C_{44} as outlined in Equation 2, are regarded as key constants to fulfil the criteria for cubic stability.

$$C_{11} > 0, C_{44} > 0, C_{11} - C_{12} > 0, C_{11} + 2C_{12} > 0 \tag{2}$$

The shear elastic coefficient (C′) is a useful metric for evaluating phase transition's prospect at 0 K, and thus phase stability, with its calculation provided in Equation 3.

$$C' = \left(\frac{C_{11} - C_{12}}{2}\right) \tag{3}$$

The investigated B2 compositions, including pure $Ti_{50}Ru_{50}$ and $Ti_{50}Ru_{50-x}Pd_x$ with Pd content below 31.25 at. %, exhibit mechanical stability as guided by Born-Huang's theory of cubic crystals, as demonstrated by the elastic constants in Fig. 2. Above 31.25 at. % $C' < C_{11}$, demonstrating that mechanical stability decreases as a crystal approaches phase transition [25].

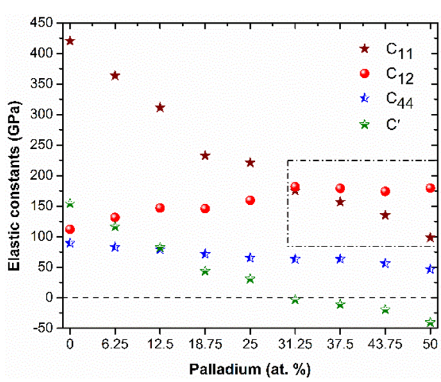

Fig. 2. Elastic properties of the studied B2 compounds

Fig. 2 further shows that ternary compounds with Pd compositions ≥ 31.25 at. % did not satisfied the mechanical stability criteria ($C_{11} < C_{12}$) resulting in C' being negative. The aforementioned signifies that the B2 phases of these ternary compositions will become unstable and likely undergo martensite transformation at lower temperatures. Given the high-temperature properties of PGMs, their presence in these ternary compositions renders them suitable for high-temperature shape memory alloy (HTSMA) applications, a trend similarly observed in Nitinol [26].

To predict mechanical properties, structural materials are characterized by elastic moduli, including shear, bulk, Young's, and Poisson's ratio, derivable from three elastic constants (C_{ij}) using the Voigt-Reuss-Hill method [24], as formulated in Equation 4 for cubic crystals.

$$B_V = B_R = \frac{1}{3}(C_{11} + 2C_{12}),\ G_V = \frac{1}{5}(C_{11} - C_{12} + 3C_{44}),\ G_R = \frac{5(C_{11} - C_{12})C_{44}}{4C_{44} + 3(C_{11} - C_{12})}, \tag{4}$$

Accordingly, bulk (B) and shear (G) are calculated as average values of $B = (B_V + B_R)/2$ and $G = (G_V + G_R)/2$, and Young's (E) and Poisson's (v) ratios are derived from $E = 9GH/(G+3B)$ and $v = (3B - E)/6B$, respectively. Bulk and shear moduli measure resistance to volume and shear deformation [27].

Material Young's modulus provides information about its stiffness, indicative of whether the material will deform easily or not [27-28]. Hardness is another key indicator of mechanical stability, measuring the resistance of solid materials to plastic deformation and permanent damage [29]. Using DFT-based first-principles methods, material properties like crystal hardness can be reliably calculated, with empirical Vickers hardness estimates obtained through the expression provided in Equation 5 [29].

$$H_V = 0.92\left(G/B\right)^{1.137} \times G^{0.708} \tag{5}$$

Pugh's and Poisson's ratios offer a framework for understanding the interatomic bonding-physical property relationship. Pugh's ratio categorizes materials as ductile or brittle based on the B/G threshold (1.75) [30], whereas Poisson's ratio identifies bond types, with values above 1/3 indicating metallic, ductile bonds [27-31].

Fig. 3 (a) – (f) presents the moduli and their corresponding ratios reported in this study. In Fig. 3(a), the stable $Ti_{50}Ru_{50}$ exhibits strong resistance to crystal deformation and atom mobility, as indicated by its larger *B, G* and *E* values.

However, as more malleable Pd atoms replace brittle Ru atoms, the stiffness of the stable $Ti_{50}Ru_{50}$ weakened, this can be indicated by the notable decay of the modulus as represented in Fig. 3 (a). As a known factor, hardness characterizes material's resilience against deformation in terms of providing the ductility or brittleness behaviour of a material [32]. It can be noted in Fig. 3 (d), that there is a sharp drop in the Vickers hardness measurement at Pd composition above 12.5 at. %, accompanied by a softening observed in *G* and *E*.

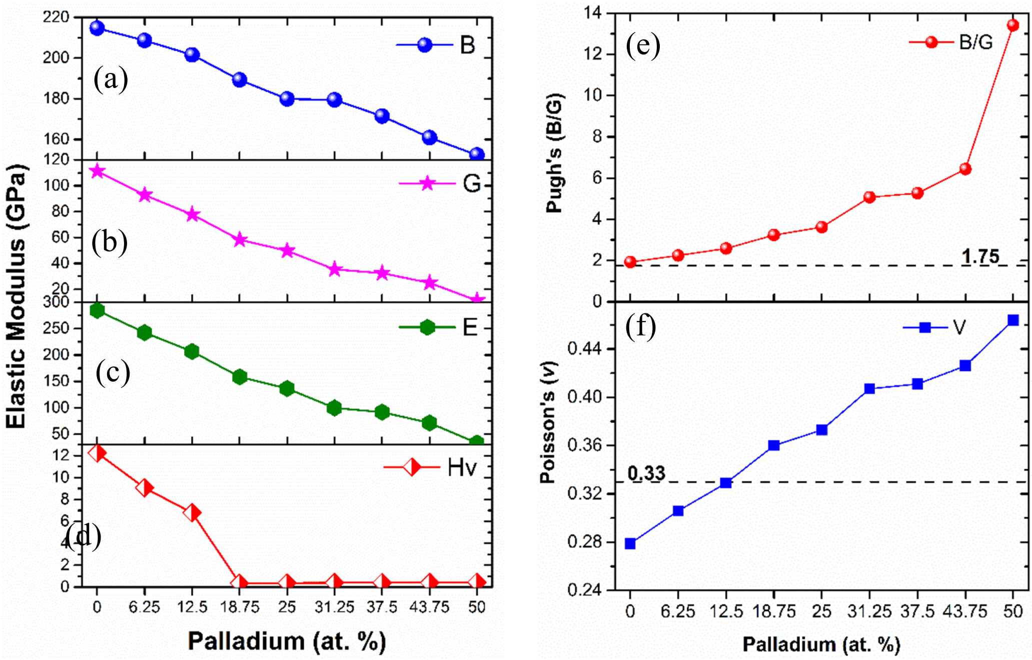

Fig. 3. The modulus of elasticity and their subsequent ratios of all the investigated B2 compounds.

Fig. 3(e) – (f) shows the Pugh's and Poisson's ratios reported in this research work. The investigated compounds demonstrate ductile properties, as evidenced by their B/G ratios, which consistently exceed the threshold value of 1.75, as shown in Fig. 3(e). However, this observation contradicts the well-known brittleness of the $Ti_{50}Ru_{50}$ compound [11, 26], its Pugh ratio should be lower than 1.75. The research by Phasha *et al.* suggests that Pugh's ductility ratio threshold of 1.75 is more effective for predicting FCC crystal structures compared to BCC structures, as observed in the B2 TiRu compound examined in this study [33].

To mitigate the above discrepancy, this study examined the bonding behaviour of investigated compounds by assessing their corresponding Poisson ratio. The results shown in Fig. 3 (f), indicate stable B2 $Ti_{50}Ru_{50}$ and ternary compounds with Pd composition under 12.5 at. % has a Poisson ratio of less than 0.33, indicating brittle ionic/covalent [28-31]. On the other hand, the ternaries with Pd composition exceeding 12.5 at. %, have a Poisson ratio greater than 0.33 indicating ductile metallic bonds.

From the mechanical stability perspective, the conclusion is to induce the shape memory effect from the stable B2 TiRu system, the Pd composition of the ideal ternary compound should not be less than 31.25 at. %.

3.3 Phonons properties

The collective vibrations of atoms in crystal lattices, known as phonons, play a crucial role in understanding the properties of crystalline materials, including thermal conductivity, mechanical strength, phase transitions, and superconducting behaviour [34]. Considering that phonons are directly linked to the dynamic behaviour of the crystal lattice during phase transitions, they are essential for evaluating compounds expected to have shape memory effects [34-36]. The phonon dispersion curves were examined and reported to provide the stability of the crystal structures investigated in this study.

A necessary condition for stability at 0 K is attained in the presence of the positive frequencies along high-symmetry paths in the Brillouin zone. While the presence of soft modes or negative frequencies, signifies dynamic instability, implying a tendency towards phase transformation accompanied by lattice deformation [7, 34-36].

Fig. 4 (a) – (i) graphically presents the sets of phonon dispersion spectra determined at room temperatures for all the investigated B2 compounds. As shown in Fig. 4(a-d), the phonon spectra of B2 $Ti_{50}Ru_{50}$ and ternary compounds with Pd content below 25 at. % display solely positive vibrational frequencies, characterized by red oscillating bands. Indicating the introduction of Pd atoms onto the Ru-site of the $Ti_{50}Ru_{50}$ compound does not yield any MT.

Furthermore, Fig. 4 (e) – (i) reveals that replacing Ru with Pd atoms above 25 at. % in B2 $Ti_{50}Ru_{50}$ triggers a significant change in vibrational dynamics. The presence of negative vibrational frequencies (blue oscillating bands) in ternary compounds with high Pd content (> 25 at. %) implies martensitic transformation properties similar to Nitinol.

The vibrational stability trends enable the authors to conclude that to induce the shape memory effect from the stable B2 TiRu system, the Pd composition of the ideal ternary compound should not be less than 31.25 at. %.

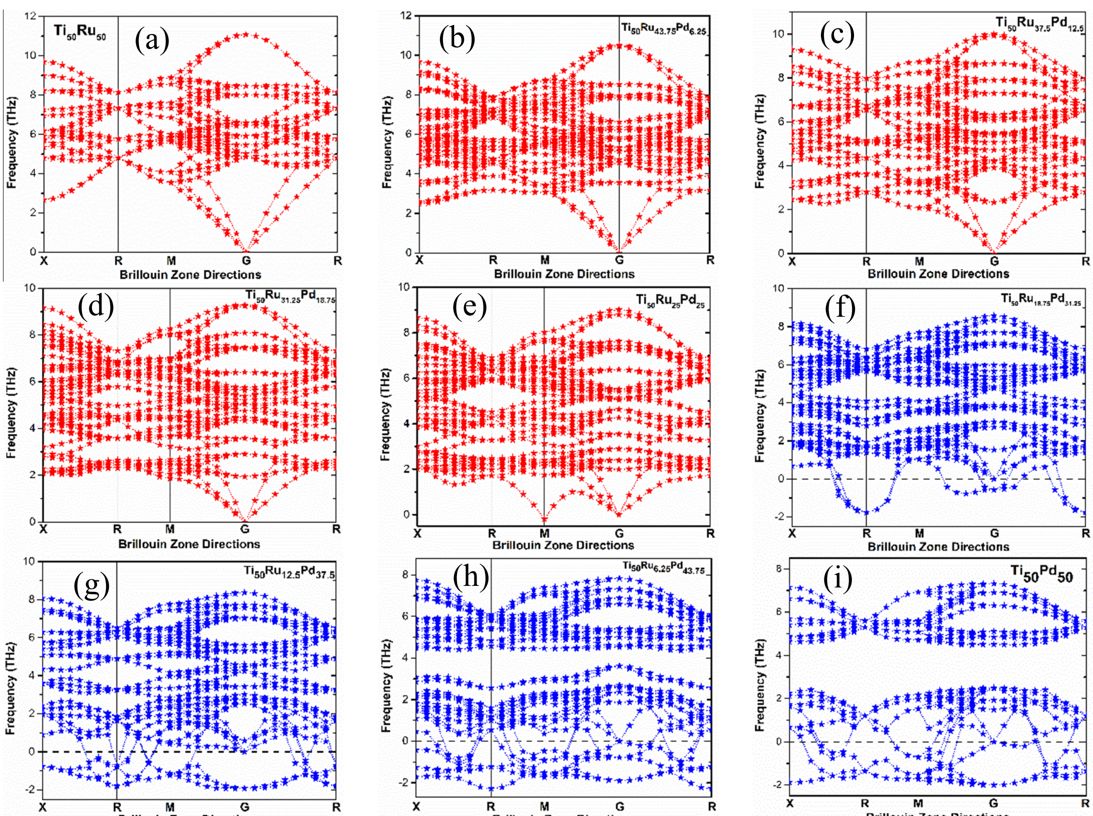

Fig. 4. Computed phonon dispersion spectra of the B2 binary and $Ti_{50}Ru_{50-x}Pd_x$ ternary alloy compositions investigated.

4 Conclusions

The thermodynamic, mechanical, and lattice dynamic characteristics of binary and ternary compounds were determined using first-principles computational techniques.

Lattice parameters and heat of formation of binary $Ti_{50}Ru_{50}$ and $Ti_{50}Pd_{50}$ reported here showed a minor variation of about 3% compared to other authors' work, which is considered acceptable. This demonstrates the accuracy of the computational parameters used, providing confidence in computing other properties. This study's calculated enthalpies of formation reveal that substituting Ru with Pd atoms reduces the thermodynamic stability of the B2 $Ti_{50}Ru_{50}$ phase. The observed linear relationship with the ternary's crystal volume expansion can be attributed to Pd atoms having a larger atomic radius compared to Ru atoms.

From a mechanical stability perspective, binary $Ti_{50}Ru_{50}$ and ternary $Ti_{50}Ru_{50-x}Pd_x$ compounds with Pd content less than 31.25 at. % fulfilled the Born-Huang stability criteria ($C'>0$). However, at Pd composition $\geq$ 31.25 at. %, C' became negative indicating phase instability with a potential martensitic transformation. Similarly, the predicted lattice dynamics results verified the instabilities of the predicted B2 ternaries at Pd compositions $\geq$ 31.25 at. %, revealing negative frequencies.

The perspective of phase, mechanical, and lattice dynamic stability investigated in this study provided insight into the phase stability/instability of the compound studied and the subsequent effect of the doping elements in inducing MT on ordered $Ti_{50}Ru_{50}$ alloy. Through systematic substitution of Ru with Pd atoms, ab initio calculations reveal the possibility of inducing martensitic phase transformation in stable B2 TiRu compounds, thereby identifying novel ternary compounds with potential shape memory properties.

The authors wish to express their gratitude to MINTEK and the University of the Witwatersrand for granting permission to share this research. They also acknowledge the financial support provided by the Advanced Materials Initiative (AMI) of the Department of Science and Innovation (DSI). Additionally, the authors thank the Centre for High-Performance Computing (CHPC) in Cape Town for access to their remote computing resources, which enabled the calculations.

References

1. A. Wadood, HEC, 1-144 (2018)
2. M.-S. Kim, J.-K. Heo, H. Rodrigue, H.-T. Lee, S. Pane, M.-W. Han, S.-H. Ahn, Adv. Mater. **35**, 1-22 (2023)
3. H. Donkersloot, J. V. Vucht, J. Less-Common. Met. **20**, 83-91 (1970)
4. J.M. Jani, M. Lervy, A. Subic, M.A. Gibson, Mater. Des. **56**, 1078-113 (2014)
5. S.E. Kulkova, D.V. Valujsky, J. Phys. IV **11**, 53-58 (2001)
6. S.E. Kulkova, D.V. Valujsky, J. S. Kim, G. Lee, Y.M. Koo, Solid State Commun. **119**, 619-623 (2001)
7. Z.Z. Kong, Y.H. Duan, M.J. Peng, D.Y. Qu, L.K. Bao, Physica. B: Cond. Matter. **573**, 13-21 (2019)
8. V. Khachin, Rev. Phys. Appl. **24**, 733-739 (1989)
9. W. Bao, D. Liu, Y. Duan, M. Peng, Philos. Mag. **99**, 1-22 (2019)
10. B.S. Ngobe, M.J. Phasha, M.P. Molepo, MRS Adv. **8**, 645-650 (2023)
11. B.S. Ngobe, M.J. Phasha, I.A. Mwamba, SAJST **40**, 205-211 (2021)
12. B.S. Ngobe, M.J. Phasha, M.P. Molepo, Y. Yamabe-Mitarai, Proc. SAIP2023, ISBN: **978-0-7961-3774-6**, 549-555 (2023)
13. B. Ngobe, M. Molepo, M. Phasha, MATEC Web Conf., **388**, 1-10 (2023)
14. M.D. Segall, J.D.L. Philip, M.J. Probert, C.J. Pickard, P.J. Hasnip, S.J. Clark, M.C. Payne, J. Phys. D: Condens. Matter. **14**, 2717-2744 (2002)
15. S.J. Clark, M.D. Segall, C.J. Pickard, P.J. Hasnip, M.J. Probert, K. Refson, M.C. Payne, Z. Kristallogr. **220**, 567-570 (2005)
16. P.E. Blöchl, Phys. Rev. B **50**, 17953-17978 (1994)
17. J.P. Perdew, Y. Wang, Phys. Rev. B **45**, 13244-13249 (1992)

18. T. Fischer, J. Almlof, J. Phys. Chem. **96**, 9768-9774 (1992)
19. J. Yang, J.H. Huang, Z. Ye, D.Y. Fan, S.H. Chen, Y. Zhao, Ceram Int. **43**, 7751-7761 (2017)
20. E. Semenova, Powder. Metall. MCeram **36**, 394-404 (1997)
21. J. Jung, G. Ghosh, G. Olson, Acta Mater. **51**, 6341-6357 (2003)
22. W.W. Xing, X. Q. Chen, D.Z. Li, L.Y. Li, C.L. Fu, Intermetallics. **28**, 16-24 (2012)
23. M. Wagner, W. Windl, Acta Mat. **56**, 6232-6245 (2008)
24. O. Gomisa, F.J. Manjónb, P. Rodríguez-Hernándezc, A. Muñozc, J.Phys. Chem. Solid. **124**, 111-120 (2019)
25. P. Sedlák, M. Janovská, L. Bodnárová, O. Heczko, H. Seiner, Metals **10**, 1-13 (2020)
26. M. Tsuji, H. Hosoda, K. Wakashima, Y. Yamabe-Mitarai, MRS Symp. Proc. **753**, BB5.52.1-BB5.52.6 (2023)
27. J. Zhang, C. Mao, C.G. Long, J. Chen, K. Tang, M.J Zhang, P. Peng, JMA **3**, 127-133 (2015)
28. E. Jain, G. Pagare, S.S. Chouhan, S.P. Sanyal, Intermetallics **54**, 79-85 (2014)
29. J. Yun-Fei, Y. Xiang-Xi, L. Jing-Tian, Z. Wen-Xian, Z. Jun, N. Xi-Jing, Chinese Phys. Lett. **27**, 076201- 076203 (2010)
30. L. Liu, X. Wu, R. Wang, X. Nie, Y. He, X. Zou, Cryst. **7**, 1-10 (2017)
31. D. Chen, Z. Chen, Y. Wu, M. Wang, N. Ma, H. Wang, Comp. Mater. Sci. **91**, 165-172 (2014)
32. J.H. García, J.C. Hernández, J. Mat. Sci. Eng. **3**, 31-34 (2016)
33. M.J. Phasha, P.E. Ngoepe, H.R. Chauke, D.G. Pettifor, D. Nguyen-Mann, Intermetallics. **13**, 2083-2089 (2010)
34. A. Togo, I. Tanaka, Scri. Mater. **108**, 1-5 (2015)
35. L. Si, Z.-Y. Jiang, B. Zhou, W.-Z. Chen, Phys. B **407**, 347-351 (2012)
36. J. Li, X. Wu, N. Bai. J. Alloy Compd. **976**, 1-9 (2024)